JGR Biogeosciences

RESEARCH ARTICLE
10.1029/2019JG005161

Special Section:
Biogeochemistry of natural organic matter

Glacier Outflow Dissolved Organic Matter as a Window Into Seasonally Changing Carbon Sources: Leverett Glacier, Greenland

A. M. Kellerman[1], J. R. Hawkings[1,2,3], J. L. Wadham[3], T. J. Kohler[4], M. Stibal[4], E. Grater[1], M. Marshall[3], J. E. Hatton[5], A. Beaton[6], and R. G. M. Spencer[1]

[1]Department of Earth, Ocean, and Atmospheric Science, Florida State University, Tallahassee, FL, USA, [2]German Research Centre for Geosciences GFZ, Potsdam, Germany, [3]Bristol Glaciology Centre, School of Geographical Sciences, University of Bristol, Bristol, UK, [4]Department of Ecology, Faculty of Science, Charles University, Prague, Czechia, [5]School of Earth Sciences, University of Bristol, Wills Memorial Building, Bristol, UK, [6]Ocean Technology and Engineering Group, National Oceanography Centre, Southampton, UK

Abstract The Greenland Ice Sheet is losing mass at a remarkable rate as a result of climatic warming. This mass loss coincides with the export of dissolved organic matter (DOM) in glacial meltwaters. However, little is known about how the source and composition of exported DOM changes over the melt season, which is key for understanding its fate in downstream ecosystems. Over the 2015 ablation season, we sampled the outflow of Leverett Glacier, a large land-terminating glacier of the Greenland Ice Sheet. Dissolved organic carbon (DOC) concentrations and DOM fluorescence were analyzed to assess the evolution of DOM sources over the course of the melt season. DOC concentrations and red-shifted fluorescence were highly associated ($R^2 > 0.95$) and suggest terrestrial inputs from overridden soils dominated DOM early season inputs before progressive dilution with increasing discharge. During the outburst period, supraglacial drainage events disrupted the subglacial drainage system and introduced dominant protein-like fluorescence signatures not observed in basal flow. These results suggest that subglacial hydrology and changing water sources influence exported DOC concentration and DOM composition, and these sources were differentiated using fluorescence characteristics. Red-shifted fluorescence components were robust proxies for DOC concentration. Finally, the majority of DOM flux, which occurs during the outburst and postoutburst periods, was characterized by protein-like fluorescence from supraglacial and potentially subglacial microbial sources. As protein-like fluorescence is linked to the bioavailability of DOM, the observed changes likely reflect seasonal variations in the impact of glacial inputs on secondary production in downstream ecosystems due to shifting hydrologic regimes.

Key Points:
- Dissolved organic carbon concentrations can be estimated in glacial outflow from the fluorescence intensity of red-shifted fluorescence
- Optical tracers can be used to differentiate subglacial from supraglacial inputs
- Optical properties in July highlight microbial sources of dissolved organic matter, with implications for downstream bioavailability

Supporting Information:
- Supporting Information S1
- Data Set S1

Correspondence to:
A. M. Kellerman,
akellerman@fsu.edu

Citation:
Kellerman, A. M., Hawkings, J. R., Wadham, J. L., Kohler, T. J., Stibal, M., Grater, E., et al. (2020). Glacier outflow dissolved organic matter as a window into seasonally changing carbon sources: Leverett Glacier, Greenland. *Journal of Geophysical Research: Biogeosciences*, *125*, e2019JG005161. https://doi.org/10.1029/2019JG005161

Received 21 MAR 2019
Accepted 28 NOV 2019
Accepted article online 6 MAR 2020

1. Introduction

Glacial systems are potentially significant sources of bioavailable dissolved organic matter (DOM) to downstream aquatic ecosystems (Fellman et al., 2010; Hood et al., 2009; Singer et al., 2012; Spencer et al., 2014). In the Arctic, DOM and other nutrients exported from the Greenland Ice Sheet (GrIS) may subsidize primary and secondary production in coastal ecosystems (Bhatia et al., 2013; Hawkings et al., 2014; Hawkings et al., 2016; Lawson, Wadham, et al., 2014; Wadham et al., 2016). The GrIS stores an estimated 0.22 Pg of dissolved organic carbon (DOC), with an estimated annual flux of 0.22 ± 0.04 Tg C year^{-1}, equivalent to one sixth of the annual DOC flux from the Yukon River (Hood et al., 2015; Spencer et al., 2013). Between 1992 and 2011, the GrIS lost an average 142 ± 49 Gt year^{-1} of mass (Shepherd et al., 2012), and in 2012, ice mass loss equated to ~574 Gt, equivalent to 1.2 mm of sea level rise (Tedesco et al., 2013; van den Broeke et al., 2016). Ice mass loss and associated meltwater runoff are likely to see rapid increases in the coming decades (Trusel et al., 2018), which may have significant implications for the downstream export of DOM.

DOM is a heterogeneous mixture of nonliving organic molecules ultimately sourced from autotrophic production and is a central component of the global carbon cycle (Hansell et al., 2009; Hedges, 1992). Sources of DOM in glacial outflow potentially originate from a variety of sources depending on the climatic and historical conditions. Previous studies have noted these may include subglacial sources from overridden soils and vegetation and/or microbial production (Bhatia et al., 2013; O'Donnell et al., 2016; Wadham et al.,

2008), supraglacial microbial production (Musilova et al., 2017; Remias et al., 2012; Smith et al., 2017; Smith et al., 2018), and supraglacial deposition (Singer et al., 2012; Spencer et al., 2014; Stubbins et al., 2012). Overridden soils and vegetation are a potentially important source of DOM along the southwestern margin of the GrIS, where the margin of the ice sheet retreated back from its current position during the Holocene Thermal Maximum (Lecavalier et al., 2014; Levy et al., 2017). Alternative subglacial sources to overridden soils and vegetation might include lithogenic DOM (Petsch et al., 2001; Petsch et al., 2005), chemolithoautotrophic production of DOM (Birdwell & Engel, 2009; Chen et al., 2009; Harrold et al., 2015), and the reworking of existing DOM by subglacial microbial communities (Cameron et al., 2017; Lamarche-Gagnon et al., 2019; Stibal et al., 2012).

The GrIS is polythermal and therefore largely underlain by liquid and frozen subglacial (or basal) water (Jordan et al., 2018; MacGregor et al., 2016). Subglacial sources of DOM are likely to be most influential on the composition of DOM when subglacial waters comprise a dominant fraction of the meltwater (Spencer, Vermilyea, et al., 2014). The hydrological evolution of glaciers that terminate on the southwestern margin of the GrIS is similar to that of temperate glaciers, whereby drainage characteristics evolve from inefficiently drained, long-residence-time basal water-dominated systems at the onset of melt to efficient systems primarily draining supraglacial meltwater during the progression of the melt (ablation) season (Bartholomew et al., 2011; Bhatia et al., 2011; Chandler et al., 2013).

Glacial outflow exhibits DOC concentrations generally <0.5 mg C L^{-1}, and seasonal sampling at the southwestern margin of the GrIS has shown either a seasonal decrease in DOC concentration (Bhatia et al., 2013) or no discernible seasonal trend in DOC concentration (Lawson, Wadham, et al., 2014). DOC concentrations are relatively high in the marginal basal ice of Leverett Glacier (LG) compared to outflow (Lawson, Wadham, et al., 2014), and DOC concentrations in the interior subglacial environment are largely unknown. Supraglacial systems exhibit a wide range of DOC concentrations. For example, cryoconite holes and dirty ice (1.6 ± 2.5 mg C L^{-1}, $n = 99$) can exhibit DOC concentrations an order of magnitude more concentrated than the dilute snow and supraglacial melt (0.2 ± 0.2 mg C L^{-1}, $n = 52$) that drains through moulins and crevasses (Holland et al., 2019; Lawson, Wadham, et al., 2014; Musilova et al., 2017). Thus, with a seasonal progression from basal-dominated to supraglacial-dominated inputs (Bhatia et al., 2013), DOC concentrations are expected to decrease with increasing discharge.

DOM optical properties have been used to delineate DOM sources and reactivity in a host of past studies on nonglacial systems (as reviewed in Fellman et al., 2010). Protein-like fluorescence has been found to dominate DOM in glacial environments (Barker et al., 2013; Dubnick et al., 2017; Fellman, Spencer, et al., 2010; Hood et al., 2009) and has been linked to high DOC bioavailability in mountain glaciers (Hood et al., 2009; Singer et al., 2012). Elevated DOC bioavailability has also been observed in GrIS outlet glaciers (Lawson, Wadham, et al., 2014; Paulsen et al., 2017), but studies examining the temporal evolution of DOM composition in glacial outflow from the GrIS using high-resolution mass spectrometry have either shown increasing terrestrial inputs or no seasonal trend in DOM composition (Bhatia et al., 2010; Lawson, Bhatia, et al., 2014). Thus, the sources and composition of DOM exported from large meltwater rivers draining the GrIS, and how the contributions may shift from different DOM sources over the course of a melt season, are largely unconstrained. This study is the first at this site utilizing fluorescence spectroscopy to assess the seasonal evolution of DOM characteristics and sources in glacial outflow at a high temporal resolution.

LG in southwest Greenland is a relatively large (~600 km^2) land-terminating outlet glacier of the GrIS. The seasonal evolution of the LG drainage system is punctuated by several large hydrological perturbation events, commonly referred to as "outburst events," where ponded supraglacial meltwater rapidly drains through the ice and flushes stored subglacial waters (Bartholomew et al., 2011; Hatton et al., 2019; Nienow et al., 2017). LG exhibits a seasonal progression in the flux of particulate organic carbon, which increases with the suspended particulate matter (SPM) load, reaching its maximum during the outburst period (Kohler et al., 2017). This is in contrast to the flux of DOC, which increases into the outburst period and remains comparatively high throughout the postoutburst period (Kohler et al., 2017), suggesting there may be a significant supraglacial or subglacial microbial source of DOM in glacial meltwater.

To assess whether DOM exported from the southwestern GrIS exhibits a seasonal evolution in source, samples were collected every 1 to 3 days from 12 May to 29 July 2015, from the proglacial river of LG (Figure 1). We examined changes in DOC concentration in conjunction with DOM fluorescence characteristics. We

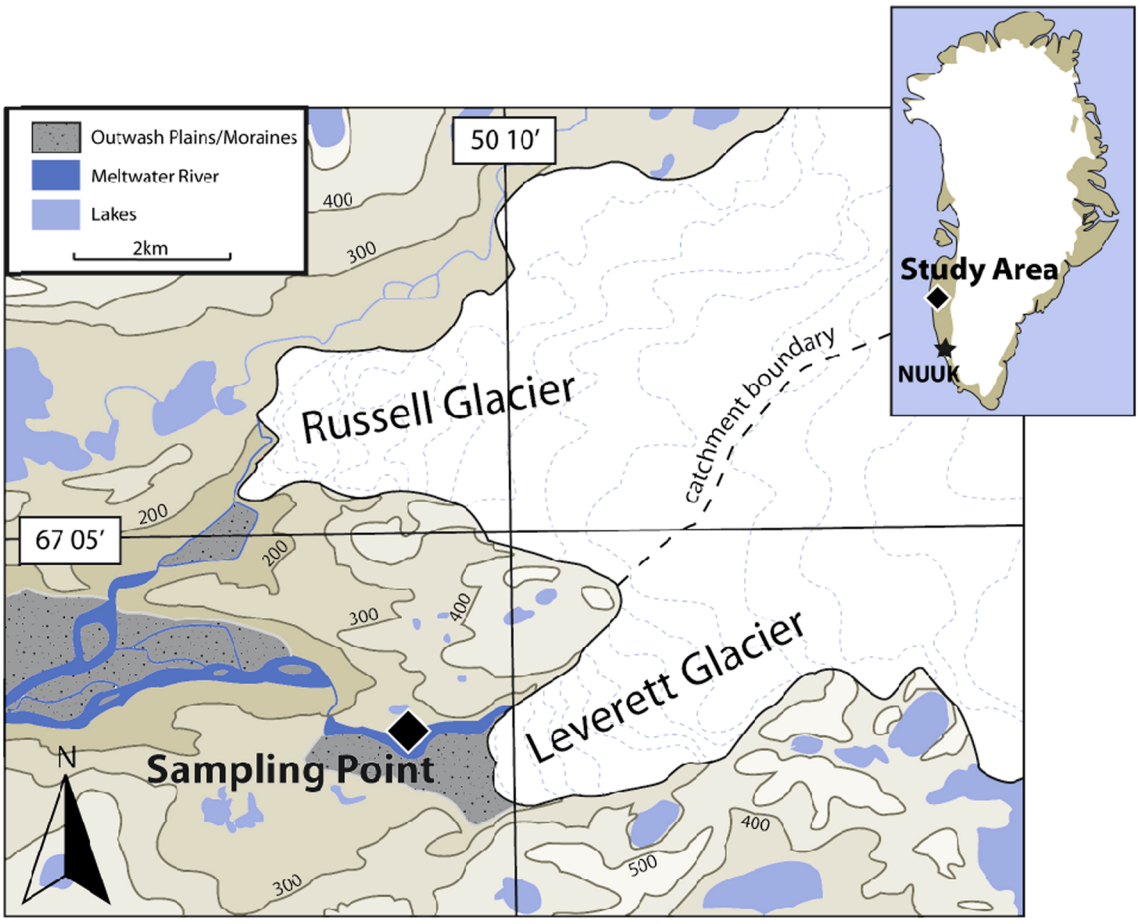

Figure 1. Map of the sampling location of Leverett Glacier outflow. Leverett Glacier is located on the southwestern side of the Greenland Ice Sheet. The boundary of the ~600 km^2 catchment is demarcated by the dashed line (Cowton et al., 2012). The sampling location is marked by the black filled circle approximately 1 km downstream from the Leverett Glacier portal. Adapted from Hawkings et al., 2014.

hypothesized that concurrent with increasing discharge as the melt season progresses, DOC concentrations would decrease and DOM fluorescence characteristics would begin to reflect supraglacial sources as the outflow shifts from subglacial- to supraglacial-dominated source waters. However, flux of DOC increases into the melt season as the increase in discharge outweighs the decrease in DOC concentration. We assess shifting flow paths through commonly used hydrological and geochemical tracers, including discharge, specific conductivity, pH, and SPM (Bartholomew et al., 2011; Hatton et al., 2019; Nienow et al., 2017). Finally, we interpret the changing composition of DOM from the outflow of LG in the context of subglacial (basal ice) and supraglacial end-members (snow) to delineate dominant inputs throughout the season.

2. Materials and Methods

2.1. Sampling Site and Catchment Characteristics

LG drains from a single portal on the northern side of the terminus and covers a hydrologically active catchment of ~600 km^2 extending >50 km into the ice sheet interior (Cowton et al., 2012). Samples were collected approximately 1.5 km downstream from the outflow at the glacier portal every 1 to 3 days for a total of 47 samples between 12 May and 29 July 2015 (Figure 1) to assess the temporal variability in DOC concentration and DOM fluorescence characteristics from the outflow of LG. A final glacial meltwater sample was taken on 28 October 2015, which represents a return to winter conditions. Samples were typically collected between 10:00 and 11:00 a.m. local time (GMT−3). Although the sampling site was 1.5 km downstream

from the glacial terminus, the high discharge and turbidity make autochthonous proglacial production unlikely. Comparative samples of geochemical parameters taken in previous years at the portal and our downstream sampling site exhibited negligible differences (Hawkings et al., 2014).

Samples for DOC concentrations and DOM optical properties were filtered using 0.45 μm Whatman® GD/XP PES syringe filters into acid-washed high-density polyethylene (HDPE) bottles (10% HCl *v*/*v* for 48 hr) and kept in the dark and frozen until analysis for DOC concentration (September 2016) and DOM fluorescence (spring 2017). Samples for DOC concentration and DOM fluorescence analyses were frozen due to the remote nature and duration of the fieldwork and the high bioavailabilty previously observed in glacial outflow samples (e.g., Hood et al., 2009). Extended freezing of filtered samples with low DOC concentrations is routine and has resulted in no observable differences greater than analytical error (Spencer & Coble, 2014).

In order to compare glacial outflow composition to supraglacial and subglacial end-members, three basal ice and three snow samples were collected. Basal ice samples were extracted by chainsaw from an easily accessible outcrop of debris-rich ice at the ice margin of the Russell-Leverett catchment (67.09°N, 50.23°W) (Wadham et al., 2016). The outer ~0.5 m of ice was removed before extracting ~30 × 30 × 30 cm blocks. The ice blocks were wrapped in precombusted foil and kept frozen until processing in a clean lab environment. The outer 10–30 mm of ice was melted with ultrapure water (>18.2 MΩ cm^{-1}), and the remaining ice was transferred to a precombusted (550 °C > 5 hr) glass beaker covered with foil under a laminar flow bench. A small amount of ice (~1–5 mm) was allowed to melt, and the water was discarded, before allowing the rest of the ice block to melt. Ice melt was then filtered through a 0.45 μm syringe filter (Whatman Puradisc PP) into an acid-cleaned HDPE bottle and frozen immediately. Snow samples were collected proximal to the meltwater river sampling location (67.06°N, 50.20°W) in early May 2015 using acid-washed 1 L HDPE bottles (Nalgene®). Samples were allowed to melt and were then filtered as per meltwater samples above.

2.2. Discharge, Sample Collection, and Water Quality Parameters

The discharge (*Q*) record was constructed by creating a rating curve between stage and discharge measured using rhodamine dye traces over the full range of river stages as described in Hawkings et al. (2018). Specific conductivity (SpC), pH, and turbidity were recorded every 15 min using a Campbell data logger. Temperature-corrected SpC was measured using a Campbell Scientific 247-L electrical conductivity probe, and pH was measured using a Honeywell Durafet pH sensor. Turbidity was used to calculate SPM concentration by calibrating to daily manual measurements of SPM concentration by filtering a known quantity of meltwater through a preweighed 0.45 μm cellulose nitrate filter, oven-drying, and reweighing as described previously (Kohler et al., 2017).

Nitrate was quantified as described previously (Wadham et al., 2016) using an IonPac™ AS11-HC-4 μm anion-exchange column fitted to a Thermo Scientific Dionex ICS-5000 with a cell temperature of 35 °C. Samples were introduced with a 0.4 μl injection volume and 30 mM KOH eluent concentration. Soluble-reactive phosphorus (hereafter referred to as phosphate) was quantified using a LaChat QuickChem 8500 series 2 flow injection analyzer as described previously (Hawkings et al., 2016) using a protocol based on the molybdenum blue method. The nitrate and phosphate concentrations of field procedural blanks, which were below the detection limit of 0.08 μM N and 0.01 μM P, were subtracted from the concentrations of outflow samples.

2.3. DOC Concentration and DOM Composition Analysis

DOC concentration was measured using a Shimadzu TOC-L_{CHN} fit with a high-sensitivity catalyst. Sample concentrations were calculated from a manual calibration curve based on standards (0.05–2.50 mg C L^{-1}), gravimetrically prepared from a certified TOC standard of potassium hydrogen naphthalate (1,000 ± 10 mg C L^{-1}; Sigma Aldrich). The limit of quantification (LOQ) was 0.039 mg L^{-1} (where LOQ = LOB + 5*x* SD of low concentration sample; LOB = limit of baseline) (Armbruster & Pry, 2008). Repeat standard measurements of 0.10, 0.15, and 0.50 mg C L^{-1} had a coefficient of variance <5%.

DOM absorbance and fluorescence characteristics were measured using a Horiba Scientific Aqualog. Scans were collected over excitation wavelengths from 230 to 800 nm in 5 nm increments and emission wavelengths from 250 to 800 nm over 2.33 nm increments using a 20 s integration time. Excitation-emission

matrices (EEMs) were corrected using a blank measured with the same settings. EEMs were trimmed to an excitation range of 260–500 nm and an emission range of 300–600 nm for further analysis.

2.4. Statistical Analysis

EEMs were deconvoluted into five components using parallel factor analysis (PARAFAC) and the drEEM toolbox (Murphy et al., 2013) in MATLAB (supporting information Table S1 and Figure S1). The PARAFAC model was validated using split-half validation (supporting information Figure S2) and inspection of residuals (Murphy et al., 2013), and it explained 99.4% of the variance. The five components are as follows and abbreviated using their fluorescence emission maximum wavelengths as in Wünsch et al. (2017). The first component had excitation/emission maxima at 265 nm/317 nm (C_{317}), the second component at <260 nm and 365 nm/483 nm (C_{483}), the third component at <260 nm and 315 nm/425 nm (C_{425}), the fourth component at <260 nm and 280 nm/416 nm (C_{416}), and the fifth component at 265 nm and 300 nm/368 nm (C_{368}). Both the intensity of the component and the percent that each component makes up of the sum of the five component intensities are reported.

All other analyses were conducted in R (*R* Core Team, 2015) and using the *vegan* package (Oksanen et al., 2011). Heterogeneity of variance was not met for many variables; thus, Welch's one-way analysis of variance not assuming equal variances was employed. If the overall analysis of means was significant (p value < 0.05), pairwise comparisons were assessed, assuming unequal variances. If an R^2 value is provided in the results, the test was either a linear or exponential regression, as specified. Nonmetric multidimensional scaling (NMDS) using Bray-Curtis dissimilarity was conducted on DOC concentration and the percent of each PARAFAC component, standardized to a range of 0 to 1. Hydrological and geochemical variables were fit to the ordination over 999 permutations. NMDS was conducted to assess the variability of LG outflow DOM over the course of the melt season, to determine how DOM composition in outflow samples varied with hydrologic and geochemical variables and to compare outflow with basal ice and snow samples.

3. Results

3.1. Hydrologic Setting

Three distinct periods over the melt season were determined by the hydrologic and geochemical data: onset of melt (12 May to 19 June 2015; days of year (DOYs): 132–170), outburst period (20 June to 11 July 2015; DOYs: 171–192), and the postoutburst period (12–29 July 2015; DOYs: 193–210, i.e., end of the main sampling period). Mean daily discharge (Q), SPM concentration, and pH were significantly different across all periods when assuming unequal variances (p value < 0.05); however, SpC was only significantly different between the onset of melt and the two later periods. The onset of melt period was characterized by a gradual increase in Q from <5 to 54.6 $m^3\ s^{-1}$ (Figure 2a), high SpC, and low SPM concentrations and pH (Figure 2b and Table 1). The outburst period exhibited four distinct outburst events, characterized by rapidly rising Q and spikes in SPM and SpC (Figures 2a and 2b) (Bartholomew et al., 2011; Kohler et al., 2017), but on average, the outburst period exhibited intermediate Q and pH levels (mean ± s.d.: 193 ± 96 $m^3\ s^{-1}$ and 8.43 ± 0.44, respectively) and low SpC and high SPM (11.2 ± 2.9 $\mu S\ cm^{-1}$ and 1.11 ± 0.34 $g\ L^{-1}$, respectively; Table 1). Q reached a maximum daily mean of 360 $m^3\ s^{-1}$ during the outburst period, but in the postoutburst period, the mean Q increased (276 ± 36 $m^3\ s^{-1}$), the variability of which is dependent on weather conditions that determine the surface melt extent on the GrIS (Braithwaite, 1995; Cowton et al., 2012). The SPM was high throughout the sampling period (>0.5 $g\ L^{-1}$) and underwent sudden and distinct increases during outburst events (up to ~2.3 $g\ L^{-1}$; Figure 2b). SpC was initially high and decreased exponentially with increasing Q (Figure 3a) due to the increasing contribution of dilute surface melt, with spikes in SpC observed during outburst events (Figure 2b). pH increased significantly across the three periods (p value < 0.05) to maximum values during the postoutburst period (8.91 ± 0.47; Table 1).

Nitrate and phosphate were inversely related ($R^2 = 0.67$, p value < 0.001). Nitrate decreased significantly from 3.4 ± 0.9 μM N during the onset of melt to 1.7 ± 0.5 μM N during the outburst period and to 1.1 ± 0.3 μM N during the postoutburst period (p value < 0.001, for all comparisons). Phosphate increased significantly from onset of melt to the outburst period from 0.06 ± 0.04 to 0.19 ± 0.05 μM P (p value < 0.001), similar to trends observed in the 2012 melt season at LG (Hawkings et al., 2016); however, it did not change appreciably between the outburst and postoutburst periods (0.20 ± 0.03 μM P, p value > 0.05).

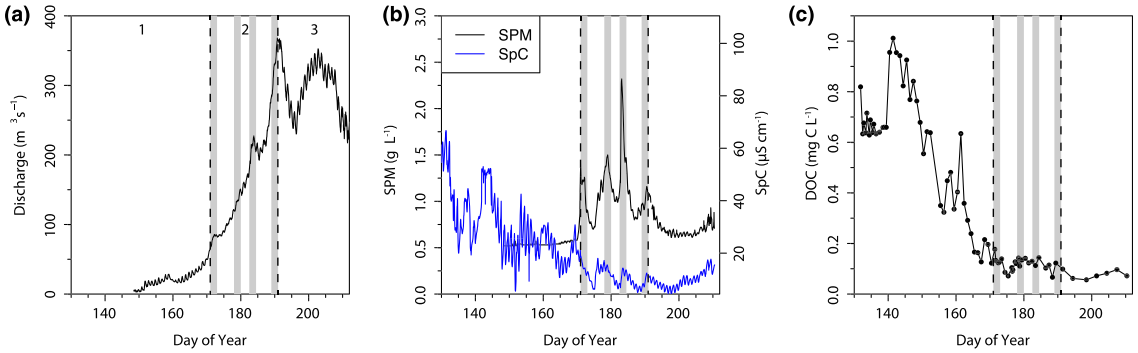

Figure 2. Hydrological and geochemical data for Leverett Glacier during the main sampling period in 2015. (a) Discharge ($m^3\ s^{-1}$), (b) suspended particulate matter concentration (SPM; $g\ L^{-1}$) and specific conductivity (SpC; $\mu S\ cm^{-1}$), and (c) DOC concentration (mg C L^{-1}). Gray vertical bars indicate outburst events. Black vertical dashed lines delineate the three sampling periods: (1) onset of melt, (2) outburst period, and (3) postoutburst period.

3.2. LG DOC Concentrations and Fluorescence Characteristics

DOC concentrations were initially high and decreased exponentially with increasing Q (Figures 2c and 3b; $R^2 = 0.89$, p value < 0.001) and decreased in a log-log fashion with decreasing SpC ($R^2 = 0.83$, p value < 0.001). DOC concentrations during onset of melt were highest and most variable (0.57 ± 0.25 mg C L^{-1}) and then decreased significantly to 0.12 ± 0.03 and 0.07 ± 0.01 mg C L^{-1} during the outburst and postoutburst periods, respectively (Table 1; p value < 0.001 for all comparisons).

The noted changes in DOC concentration were closely tracked by the changes in the five fluorescence components deconvoluted by PARAFAC modeling (see section 2 and supporting information Figure S1 and Table S1) in both their intensities and the percent changes in each component. Two components (C_{483} and C_{425}) were red-shifted with UVA and UVC humic-like fluorescence. These two components have been widely reported in the fluorescence literature and are generally thought to be derived from terrestrial sources (Fellman, Hood, & Spencer, 2010; Goncalves-Araujo et al., 2016; Kothawala et al., 2014; Osburn et al., 2016). C_{483} and C_{425} exhibit tightly linked temporal changes in intensities and the percent of fluorescence each component comprises over time (Figures 4a and 4d). C_{483} and C_{425} exhibit moderate fluorescence intensities in mid-May, before increasing concurrently with DOC concentration at the first initial meltwater pulse (days 140–143). C_{483} and C_{425} decrease significantly with each subsequent period (p value < 0.001 for each

Table 1
Hydrological, Geochemical, and Dissolved Organic Matter Data for Leverett Glacier Outflow

	Onset of melt	Outburst period	Post-outburst	Total melt	Basal Ice	Snow	October
Variable	$n = 23$	$n = 15$	$n = 9$	$n = 47$	$n = 3$	$n = 3$	$n = 1$
Hydrological and geochemical							
Q ($m^3\ s^{-1}$)	12 ± 13	193 ± 96	276 ± 36	121 ± 124			
SpC ($\mu S\ cm^{-1}$)	31.9 ± 10.0	11.2 ± 2.9	11.3 ± 3.2	21.3 ± 12.7			
SPM ($g\ L^{-1}$)	0.55 ± 0.05	1.11 ± 0.34	0.71 ± 0.06	0.82 ± 0.33			
pH	7.84 ± 0.21	8.43 ± 0.44	8.91 ± 0.47	8.24 ± 0.55			
Nitrate (µM)	3.4 ± 0.9	1.7 ± 0.5	1.1 ± 0.3	2.4 ± 1.2			
Phosphate (µM)	0.06 ± 0.04	0.19 ± 0.05	0.20 ± 0.03	0.13 ± 0.08			
DOM							
DOC (mg C L^{-1})	0.57 ± 0.25	0.12 ± 0.03	0.07 ± 0.01	0.33 ± 0.30	0.88*	NA	0.49*
Total fluorescence (R.U.)	0.96 ± 0.39	0.39 ± 0.13	0.48 ± 0.16	0.69 ± 0.40	2.60 ± 0.78	0.14 ± 0.08	0.81*
$\%C_{317}$	28 ± 9	48 ± 16	57 ± 20	35 ± 22	18 ± 2	99 ± 2	24*
$\%C_{483}$	32 ± 4	14 ± 7	6 ± 2	21 ± 12	34 ± 2	0 ± 0	31*
$\%C_{425}$	28 ± 3	16 ± 6	7 ± 2	20 ± 9	23 ± 3	1 ± 2	23*
$\%C_{416}$	12 ± 2	17 ± 19	26 ± 23	16 ± 15	9 ± 2	0 ± 0	10*
$\%C_{368}$	10 ± 4	5 ± 5	4 ± 4	8 ± 5	15 ± 4	0 ± 0	12*

*Indicates samples where no replicates were measured; NA indicates where no sample was available Q: discharge; SpC: specific conductivity; SPM: suspended particulate matter concentrations; DOC: dissolved organic carbon concentration; %Ci: fraction of fluorescence component.

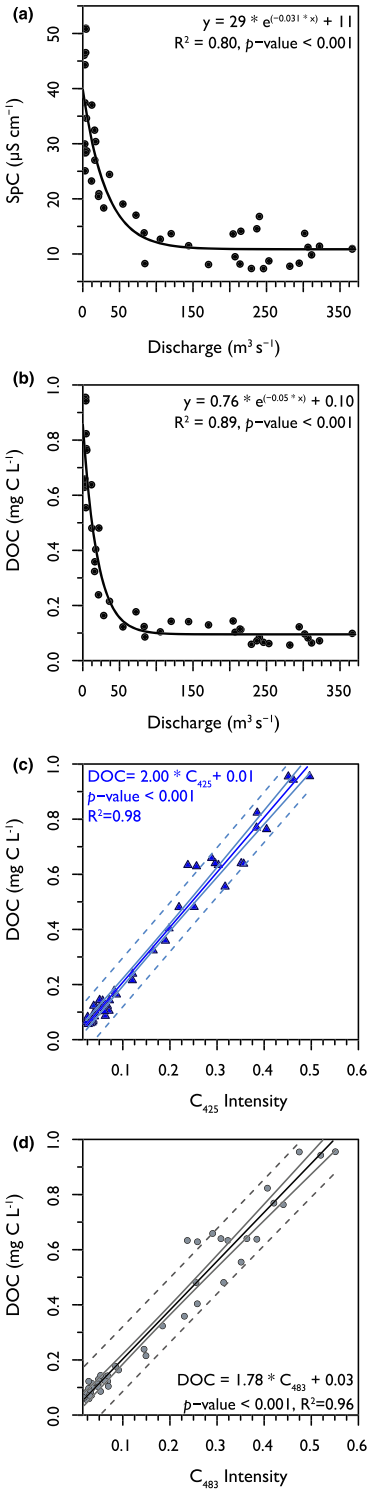

Figure 3. Associations between DOC concentration and discharge and fluorescence component intensities. (a) SpC and (b) DOC concentration decreases exponentially with increasing discharge. DOC increases linearly with the intensity of fluorescence components (c) C_{425} (blue triangles and lines) and (d) C_{483} (black circles and lines) , that is, components with signatures of plant and soil sources. Solid black and dark blue lines represent the regression, with gray and light blue solid and dashed curves indicating the 95% confidence and prediction intervals, respectively.

pairwise comparison), closely tracking the decrease in DOC concentration observed with increasing Q (Table 1). C_{483} and C_{425} are positively and significantly related to DOC concentration (Figures 3c and 3d; C_{483}: $R^2 = 0.96$, p value < 0.001; and C_{425}: $R^2 = 0.98$, p value < 0.001). C_{368}, a blue-shifted component similar to previously described tryptophan-like fluorescence (Fellman, Hood, & Spencer, 2010), exhibits temporal trends similar to those of C_{483} and C_{425} (Figure 4a and 4d). Although the component intensities decrease, the fractions of C_{483}, C_{425}, and C_{368} do not change appreciably until the outburst period (Figure 4d). During the outburst period the fraction of fluorescence that components C_{483}, C_{425}, and C_{368} comprise decreases significantly (70% ± 2% to 35% ± 2%; Table 1) and continues to decrease in the postoutburst period (18% ± 3%; p value < 0.001 for all comparisons; Table 1). This pattern is also apparent in the NMDS (Figures 5a and 5b), where the percent abundance of C_{483}, C_{425}, and C_{368} and DOC concentrations have high negative scoring on the first dimension. SpC is negatively associated with the first dimension of the NMDS, reflecting how, as SpC decreases with increasing Q, DOC concentration and the percent of C_{483}, C_{425}, and C_{368} decrease concurrently (Figure 5a).

Basal ice samples exhibited the highest total fluorescence overall, which was predominantly composed of C_{483}, C_{425}, and C_{368}, proportionally similar to the fluorescent DOM in early season outflow (Figures 4a, 4d, and 5b and Table 1). Conversely, snow samples exhibited no fluorescence for C_{483}, C_{425}, or C_{368} and exhibited the lowest fluorescence overall (Figures 4 and 5b and Table 1). Snow samples predominantly exhibited fluorescence from C_{317} (99% ± 2%, $n = 3$; Figures 4b and 4e and Table 1), similar to the previously described tyrosine-like peak (Fellman, Hood, & Spencer, 2010). The basal ice sample exhibited 18% ± 2% of fluorescence from C_{317} ($n = 3$; Figure 4e and Table 1), similar to the preoutburst levels of C_{317} in the meltwater samples. Multivariate ordination confirms there is a distinct separation between DOM composition in LG basal ice and snow (Figure 5b; NMDS1).

The DOM optical properties of LG outflow diverged from that in basal ice as C_{483}, C_{425}, and C_{368} intensities decreased exponentially with increasing Q (C_{483}: $R^2 = 0.85$, p value < 0.001; C_{425}: $R^2 = 0.86$, p value < 0.001; C_{368}: $R^2 > 0.71$, $p < 0.001$) and became more similar to the snow samples as the melt season progressed, where $\%C_{317}$ dominated the composition (Figure 4e and Table 1). This increase in C_{317} is associated with the increase in the SPM as the melt season progresses (Figure 5a and Table 1). However, the dominance of $\%C_{317}$ in the EEMs in the outburst and postoutburst periods is dependent on the stochastic presence of an additional component (C_{416}) late in the season when SPM was low and pH was high (Figure 5b). C_{416} is a red-shifted component with a high Stokes shift, or difference between the excitation and emission wavelengths, which appears very clearly during the outburst period and into the postoutburst period (Figures 4c and 4f and Table 1). A component similar to C_{416} has only been observed in two models in the OpenFluor database (Murphy et al., 2014), both of which have large influences from microbial and algal production (Osburn et al., 2016; Wünsch et al., 2017). The presence of C_{416} resulted in a group of compositionally distinct samples that were dissimilar to both basal ice and snow (NMDS2; Figure 5b). These compositionally distinct DOM signatures alternated every 1–3 days

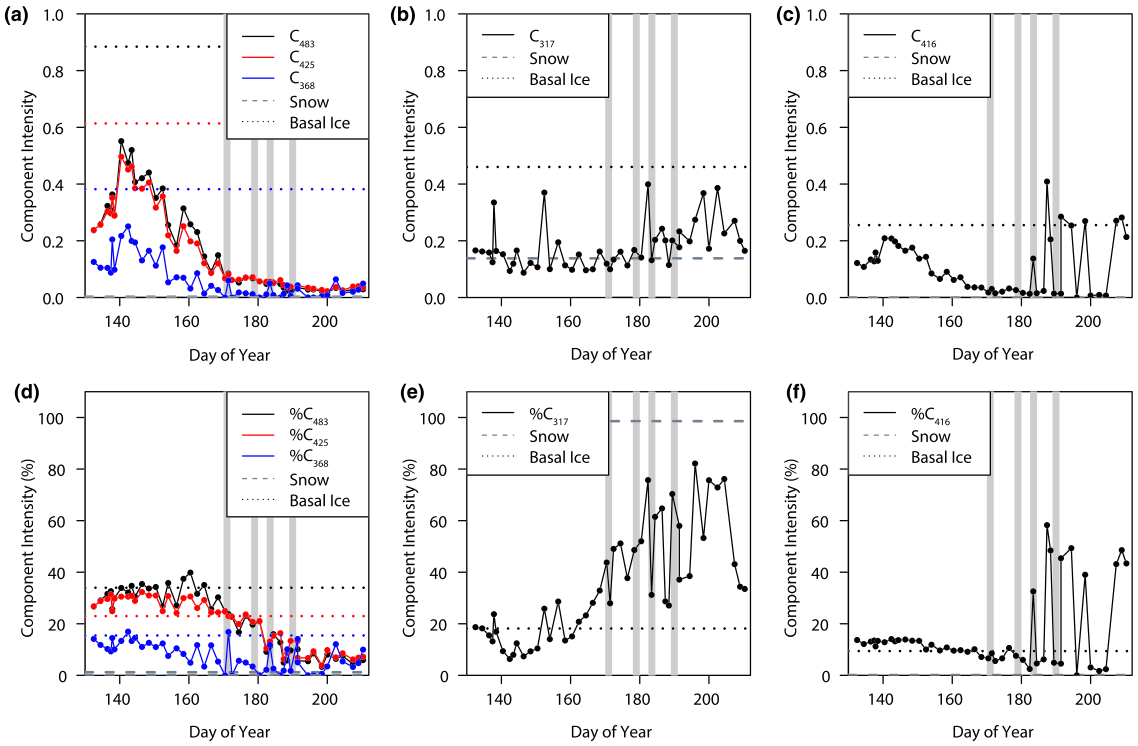

Figure 4. Time series of the fluorescence components in the outflow of Leverett Glacier over the 2015 main sampling period. (a–c) Component intensities and (d–f) component contributions are shown across the sampling period. The average ($n = 3$) intensities and contributions of each component are shown for Leverett basal ice (black, red, and blue horizontal dotted lines) and snow samples (horizontal gray dashed lines). Snow DOM fluorescence came from C_{317} (99% ± 2%); thus, dashed snow lines fall near the *y*-axes in (a), (c), (d), and (f). Gray vertical bars indicate outburst events.

throughout July (Figures 4c and 4f). By the end of October, optical properties of DOM in LG outflow had returned to that observed at the beginning of the melt season (Figure 5b), and the DOC concentration was similar to but had not quite reached that observed before the first pulse of meltwater on day 140 (0.64 ± 0.01 mg C L^{-1}, $n = 6$; vs. 0.49 mg L^{-1}, $n = 1$; Table 1).

4. Discussion

4.1. Seasonality of DOM and Fluorescence Characteristics in Glacial Outflow

Concentrations of DOC were highest early in the season when *Q* was low and SpC, $\%C_{483}$, $\%C_{425}$, and $\%C_{368}$ were high. SPM concentration and pH increased with *Q*, and DOM fluorescence typical of soil and plant sources ($\%C_{483}$ and $\%C_{425}$) decreased. Compositional variability increased over the sampling period, and by early July, C_{317} and C_{416} comprised the majority of fluorescence, with the stochastic presence of C_{416} dominating the compositional variability (Figures 4d–4f). These results suggest a model of shifting flow paths from a basal-dominated, inefficient drainage system during the onset of melt to an efficient drainage system dominated by supraglacial melt in the outburst and postoutburst periods (Figure 6). Basal sources of DOM include DOM incorporated into the basal ice, overridden paleosols, and DOM from subglacial microbial production. Supraglacial sources of DOM include deposition of organic matter, microbes, and dust, as well as supraglacial microbial and algal production. In addition to supraglacial sources, late season melt may also access DOM entrained in interior basal ice or subglacial production of DOM (Figure 6).

The similar fluorescence characteristics of basal ice and glacial meltwater samples early in the melt season demonstrate that DOM shifts from basal ice-dominated signatures to supraglacial melt, returning to basal composition by the end of October. This corresponds with the meltwater itself being dominated by long residence time basal water early in the melt season (Bhatia et al., 2011) and higher total fluorescence that has previously been observed in basal ice samples from LG (Lawson, Wadham, et al., 2014). The two components with long fluorescence emission wavelengths that are most abundant during the onset of melt are associated

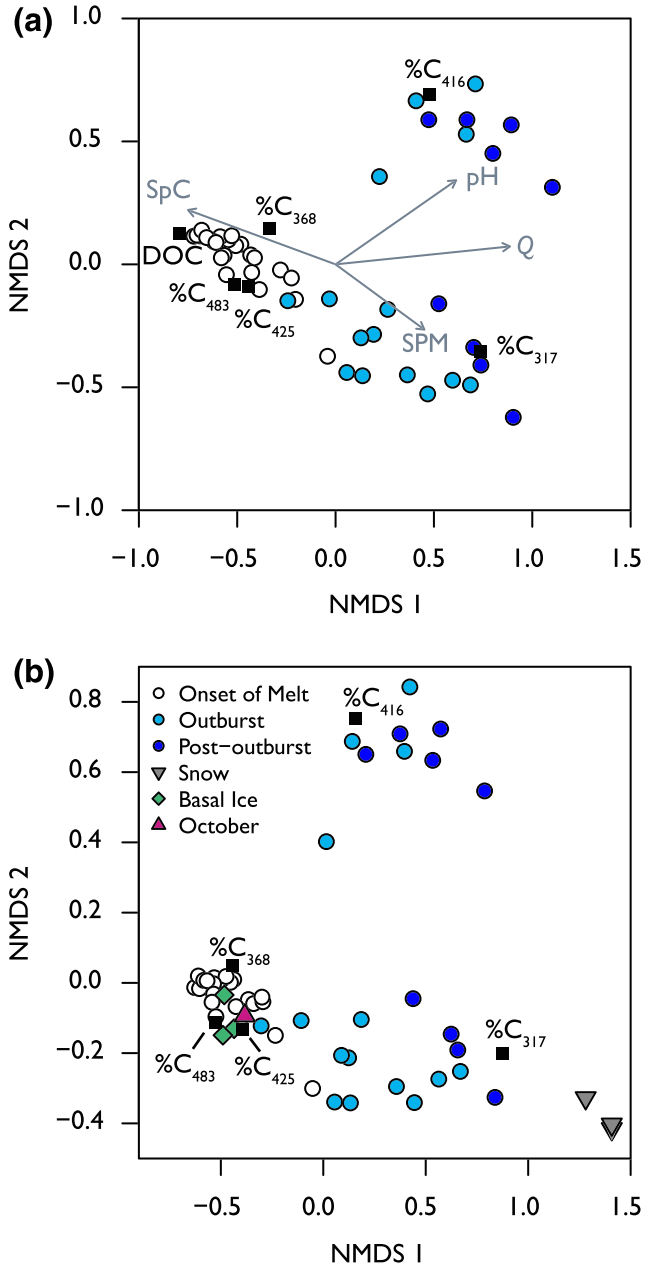

Figure 5. Nonmetric multidimensional scaling (NMDS) of DOM from Leverett glacier. (a) The first NMDS (stress = 0.04, $k = 3$) is based on fluorescence component contributions and DOC concentration. Discharge (Q), specific conductivity (SpC), pH, and suspended particulate matter concentration (SPM) were fit to the ordination (over 999 permutations), and each were significant at p value < 0.001. The color of the filled circles indicates the sampling period. (b) The second NMDS (stress = 0.03, $k = 3$) includes basal ice (green diamonds), snow (gray inverted triangles), and an LG outflow sample taken in October 2015 (pink triangle) but does not include DOC concentration.

with DOM derived from terrestrial sources (Fellman, Hood, & Spencer, 2010; Kothawala et al., 2014). Indeed, the GrIS may have retreated from 20 km to as much as 80 km inland of its present margin during the last glacial minimum ~4 kyr before present (Lecavalier et al., 2014; Levy et al., 2017; Simpson et al., 2009), allowing for the growth of vegetation and establishment of what are now overridden paleosols. DOM and particulate organic matter can then become entrained in the basal ice by ice sheet advance and freeze-on (Knight, 1997), a process by which subglacial water and sediments are integrated into the basal ice. Fluorescence indicative of terrestrial sources decreased as SPM increased (C_{483} and C_{425} semilog relationships: $R^2 = 0.30$, p value < 0.001, for both relationships), as SPM is controlled by fresh comminution of bedrock, not erosion of paleosols (Cowton et al., 2012). Particulate organic carbon concentration and SPM are correlated during the outburst and postoutburst periods (Kohler et al., 2017), when fluorescence signatures of plant and soil sources are already low. The snow line was <25 km from the ice margin during the onset of melt (Kohler et al., 2017) when fluorescence characteristics reflect soil and plant sources. This suggests that when drainage is limited to near the GrIS margin, DOM optical properties are a result of leaching from overridden paleosols or from basal ice, which has incorporated DOM from paleosols (Figure 6). The exclusion of DOM during ice formation (Belzile et al., 2002) may further enhance the export of DOM entrained in basal ice during the onset of melt.

The decrease in red-shifted fluorescence with increased melt contrasts with a previous study using ultrahigh-resolution mass spectrometry that suggested lignin-like compounds were more abundant in a GrIS proglacial stream in July than in May (Bhatia et al., 2010). This could be due to differences in the seasonal evolution of the subglacial hydrology between the two glaciers, with a potentially less developed subglacial drainage system at the smaller glacier sampled by Bhatia et al. (2010), and/or due to spatial differences in deglaciation during the Holocene Thermal Maximum, with glaciers in different regions of the GrIS incorporating varying amounts of DOM from overridden soils and vegetation. In a previous study done at LG (the same site as this study) using ultrahigh-resolution mass spectrometry, seasonal variation in DOM composition did not exhibit a clear trend over time; however, samples from the subglacial outflow reflected increased terrestrial sources relative to supraglacial samples (Lawson, Bhatia, et al., 2014). The discrepancies between the two studies may also be due to the different analytical windows of fluorescence spectroscopy and ultrahigh-resolution mass spectrometry (Kellerman et al., 2015; Martinez-Perez et al., 2017). The amount these two pools of organic matter overlap is unknown; however, polyphenolic and condensed aromatic compounds have been shown to covary with the red-shifted fluorescence of components similar to $\%C_{483}$ and $\%C_{425}$ (Kellerman et al., 2015; Kellerman et al., 2018; Stubbins et al., 2014), reflecting consistent trends despite analytical differences.

DOM from LG outflow exhibited low compositional variability early in the melt season as compared to the outburst and postoutburst periods (Figures 4d–4f and 5). Early-season DOM composition is likely due to inputs from melting basal ice that has entrained subglacial DOM or subglacial groundwater, which may be important when inputs of melting snow are limited (Beaton et al., 2017; O'Donnell et al., 2016; Spencer, Vermilyea, et al., 2014). High SpC further supports high basal connectivity during the onset of melt (Figure 3a) and, coupled with low compositional variability, indicates slow movement of water through the

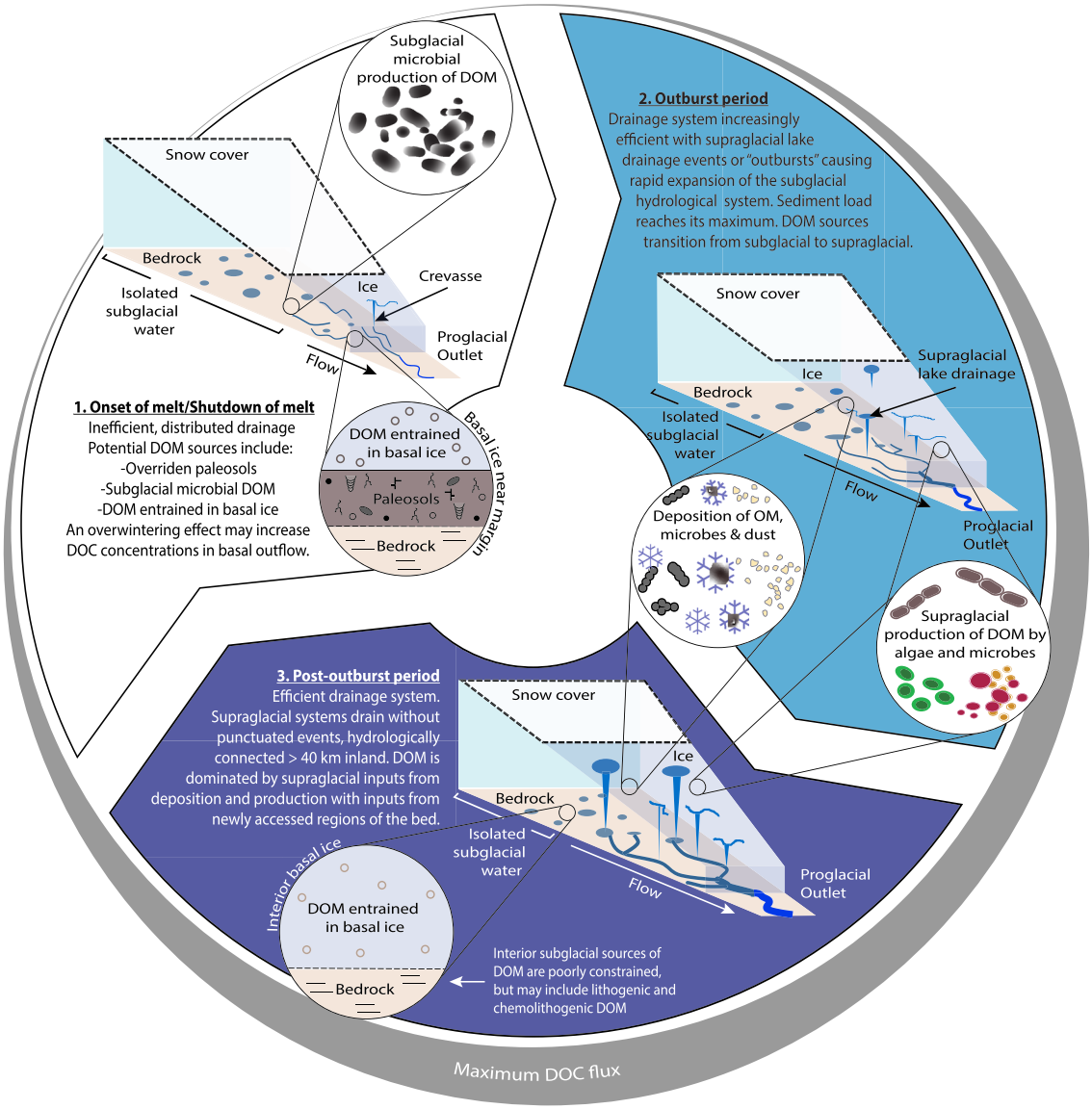

Figure 6. Conceptual diagram of the progression of the melt season and concurrent changes in DOM sources; glacier cross sections modified from Hatton et al., 2019. The white (onset of melt/shutdown of melt), light blue (outburst period), and dark blue (post-outburst period) arrows indicate the direction of the development of the melt season over the annual cycle. The gray outer band indicates the increase in DOC flux from the onset of melt to the outburst period and reaching its maximum in the postoutburst period.

inefficient drainage system. Compositional variability increases during and after the efficient drainage system is established, as the subglacial hydraulic pressure varies in the outburst and postoutburst periods (Chandler et al., 2013). An inefficient drainage system would integrate dispersed subglacial inputs into the meltwater outflow, whereas outburst events and changes in the hydraulic pressure of an efficiently drained system could rapidly change the source of DOM in glacial outflow. This has been suggested for particulate organic matter at LG, where stochastic events in the outburst period deplete subglacial particulate stocks and water pockets as the drainage system expands progressively further into the ice sheet (Kohler et al., 2017). Ultimately, while subglacial DOM may be accessed by the same mechanism as particulates, the sources are not necessarily the same. SPM concentration is a function of bedrock weathering (Cowton et al., 2012), whereas the sources and size of subglacial stores of DOM are poorly constrained.

Despite the compositional variability observed during the outburst and postoutburst periods, the DOC concentrations exhibit a small but significant decrease (Table 1). This is due to the DOC concentrations mainly being controlled by the fraction of basal inputs, with low and relatively constant DOC concentrations from supraglacial inputs. The low DOC concentrations observed in the outburst and postoutburst periods are consistent with supraglacial stream values previously reported (Musilova et al., 2017). If DOC inputs from the supraglacial environment are low and consistent, the intensity of subglacially sourced DOM ($\%C_{483}$ and $\%C_{425}$) can be used to estimate DOC concentration in glacial environments (Figure 3).

The return to basal DOM composition by the end of October reflects the shutdown of the drainage system and a return to basal-dominated DOM inputs during the end of the melt season (Figure 6). Although the October sample exhibited a DOC concentration that was higher than outflow samples during the outburst and postoutburst periods, it did not quite reach the concentrations observed before the first pulse of meltwater during the onset of melt (Table 1), suggesting either an overwintering effect may leach DOM from subglacial sediments or outflow at the onset of melt may be enriched in DOM excluded from basal ice during the winter.

4.2. Sources of Fluorescent DOM in Outflow From LG

Fluorescence that has previously been identified as "protein-like" is present in meltwater outflow as C_{317} and C_{368}. These two components exhibit similar maximum fluorescence excitation and emission wavelengths to those of the first two components in a study of DOM fluorescence across glacial samples from Antarctica, Canada, and Svalbard (Dubnick et al., 2017). Both components are present throughout the melt season, although they are inversely related. The percent contribution of C_{368} covaries with terrestrial sources ($\%C_{483}$ and $\%C_{425}$, p value ≤ 0.001, for both relationships; Figure 4d), whereas $\%C_{317}$ increases over the course of the melt season (Figure 4e). Additionally, the changes in $\%C_{368}$ and $\%C_{317}$ significantly correlate with the seasonal changes in inorganic nutrients, where $\%C_{368}$ is positively associated with nitrate ($R^2 = 0.33$, p value < 0.0001) and $\%C_{317}$ is positively associated with phosphate ($R^2 = 0.55$, p value < 0.0001). This supports a progression away from DOM sourced from soil organic matter (nitrate enriched near the glacier margin) as more remote parts of the catchment are accessed (inputs of freshly weathered subglacial phosphate-bearing minerals with increasing supraglacial melt; Hawkings et al., 2016) in the outburst and postoutburst periods. In a previous study at this site, subglacial meltwater analyzed by ultrahigh-resolution mass spectrometry suggests a high percentage of formulae assigned contain nitrogen throughout the melt season (Lawson, Bhatia, et al., 2014), which is supported by the continuous protein-like fluorescence over the melt season despite changes in contributions from different components. Protein-like fluorescence has previously been shown to covary with N-containing compounds (Kellerman et al., 2015). While protein-like fluorescence dominates the optical signatures of snow and other glacial meltwaters (Barker et al., 2013; Dubnick et al., 2017; Fellman et al., 2015), some protein-like fluorescence has been linked to the presence of lignin phenols and tannins (Hernes et al., 2009; Maie et al., 2007), which could explain the covariance between C_{368} and the components more traditionally considered to correspond with terrestrial sources (C_{483} and C_{425}). Alternatively, C_{368} may reflect production from subglacial microbial communities, which becomes diluted by increased discharge as the season progresses (Figures 4 and 6).

While C_{483} and C_{425} are typical of DOM from plant and soil sources, and C_{317} and C_{368} are similar to protein-like fluorescence, traditionally believed to be indicative of algal and microbial sources, C_{416} is a somewhat ambiguous component, with short excitation wavelengths but long emission wavelengths, and only matched two components in OpenFluor (Murphy et al., 2014). One study that described this component deconvoluted PARAFAC components from Pony Lake fulvic acid, a lake considered an end-member of microbial and algal production (Kellerman et al., 2018; McKnight et al., 2001), run on a high-pressure size-exclusion chromatograph with a fluorescence detector (Wünsch et al., 2017). The second study that described this component is from a watershed influenced by both urban and agricultural inputs (Osburn, Handsel, et al., 2016). However, C_{416} only matches these components when the Tucker's congruence criteria, an index of similarity, is set to 0.90. This suggests that C_{416} has a source of microbial origins, and that this component is rare in the fluorescence literature.

There are two potential source environments of C_{416} in LG outflow: supraglacial or subglacial. The mechanistic interpretation of the source of C_{416} is confounded by the spikes in C_{416} observed both during and after

the outburst period. The stochastic presence of C_{416} particularly during the outburst period suggests that it is a result of supraglacial production. DOM production in the GrIS supraglacial environment is dominated by glacier algae (Cook et al., 2017; Williamson et al., 2018), which can result in high DOC concentrations, despite the typically low DOC concentrations in snow (Fellman et al., 2015; Musilova et al., 2017). High discharge into moulins from supraglacial streams (Smith et al., 2015) are particularly important in the LG catchment at lower elevations (Clason et al., 2015). Above 1,000 m, supraglacial lake drainage events become increasingly important (Clason et al., 2015), and *Q* rates can change rapidly when supraglacial lakes drain from the ablation zone during the outburst period (i.e., outburst events) (Bartholomew et al., 2011; Christoffersen et al., 2018). These drainage events are characterized by rapid changes in SPM concentrations and SpC (Bartholomew et al., 2011), as stored waters at the bed are evacuated by incoming supraglacial water (Hatton et al., 2019), and thus may coincide with compositional changes in DOM in subglacial outflow. However, DOC concentrations are very low in supraglacial streams, and DOM produced by ice algae is tightly cycled through microbial respiration (Musilova et al., 2017; Smith et al., 2017) and may be retained in the weathering crust (Holland et al., 2019), making a supraglacial source of DOM unlikely to rapidly alter and dominate subglacial *Q*. Furthermore, supraglacial lake drainage events at LG only occur during the outburst period (Bartholomew et al., 2011; Kohler et al., 2017); thus, supraglacial lake drainage events cannot explain the episodic presence of C_{416} during the postoutburst period.

The second potential source of C_{416} is subglacially derived DOM either reworked or produced in situ by microbial communities. Microbial production and transformation of DOM can be through aerobic and anaerobic microbial processes (Cameron et al., 2017; Lamarche-Gagnon et al., 2019; Stibal et al., 2012). Although the LG subglacial outflow is supersaturated in oxygen, it is also supersaturated in methane (Lamarche-Gagnon et al., 2019); thus, the spatial extent of GrIS subglacial anaerobic environments is potentially vast. Water-saturated subglacial sediments are postulated to have steep redox gradients, with methanogenesis, methane oxidation, and iron and nitrate reduction observed under the GrIS (Christiansen & Jorgensen, 2018; Dieser et al., 2014; Lamarche-Gagnon et al., 2019; Yde et al., 2010).

C_{416} is only present when pH is relatively high and SPM concentration is relatively low for late-season outflow (Figure 5). The high pH observed when C_{416} is present is indicative of the hydrolysis reactions that occur when dilute meltwaters come into contact with freshly ground mineral surfaces (Hatton et al., 2019). Thus, C_{416} may have a subglacial source but is bound to particles (e.g., adsorbed to iron oxyhydroxides) when pH is low and SPM concentrations are high. Subglacial sediments are derived from the fresh comminution of bedrock, translocation of supraglacial particles, and overridden soils and vegetation (with decreasing importance). Spikes in SPM concentrations during the outburst period are a result of fresh glacial erosion, as the extremely high *Q* during outburst events lubricates the bed, speeding up the glacier and resulting in more comminution of bedrock (Cowton et al., 2012). Additionally, new subglacial sediments may be accessed and subsequently evacuated when deeper reaches of the watershed are tapped by the expanding drainage system (Kohler et al., 2017). The drainage channel may not expand rapidly enough during supraglacial lake drainage events to accommodate the water flux and results in a temporary hydraulic jacking and turbulent flow through the inefficient network near the lake (Dow et al., 2015) or a potential lapse in catchment fidelity (Lindback et al., 2015). The efficient channel may continue to expand, even after the outburst period, and new subglacial DOM may be accessed when the hydraulic pressure is low enough for water from the distributed system to drain into the efficient channel, explaining the asynchronous relationship between C_{416} and high SPM.

4.3. Implications for the Downstream Export of DOM From the GrIS

The changes in DOM composition observed over the course of the melt season confirm the dominance of distributed basal flow and groundwater during low discharge, which is characterized by high DOC concentrations and fluorescence properties indicative of overridden vegetation and soils. This is further evidenced by the fluorescence characteristics observed during the onset of melt and that observed in basal ice from the glacier margin. The fourfold decrease in $\%C_{483}$ and $\%C_{425}$ during the onset of the melt period is consistent with an expansion of subglacial drainage into the ice sheet and increasingly more efficient drainage pathways, as supraglacial input (low DOC, high $\%C_{317}$) comprises an increased fraction of meltwater as the season progresses. An increasingly protein-like fluorescence signature ($\%C_{317}$ and $\%C_{416}$) was observed as discharge increased, likely due to algal production of DOM on the surface of the GrIS and subglacial

microbial activity. There was a return to basal DOM compositional conditions by the end of October, but the DOC concentration was not yet as high as that observed in mid-May, suggesting that the overwintering of basal waters leaches DOM from sediments near the GrIS margin.

Optical tracers can be used to differentiate subglacial from supraglacial inputs, and DOC concentrations can be estimated in glacial outflow by measuring the fluorescence intensity of red-shifted fluorescence components (C_{483} and C_{425}). Although DOC concentrations decrease exponentially with increasing discharge, DOC flux increased by an order of magnitude between May and July driven by an increase in discharge by 2 orders of magnitude despite a decrease in DOC concentration by 1 order of magnitude (Kohler et al., 2017). An increase in DOC flux along with elevated contributions of potentially bioavailable DOM from algal production on the glacier surface and microbial subglacial sources, highlights the significance of mid-season C flux from glacial systems, despite the low DOC concentrations. Using the discharge-weighted mean DOC concentration (0.114 mg L^{-1}) and the total annual discharge of 1.45 km^3 (Hatton et al., 2019), the total flux of DOC from LG over the 2015 melt season is 165,000 ± 25,000 kg C $year^{-1}$. Because interannual variability in discharge is high, we used the relationship between GrIS runoff (Bamber et al., 2018) and LG *Q* (Cowton et al., 2012; Hawkings et al., 2014; Sole et al., 2013) to calculate total LG *Q* for years when no discharge record is available (Hawkings et al., 2015); the 10-year average flux of DOC from LG between 2007 and 2016 is 180,000 ± 50,000 kg C $year^{-1}$, about 3 times lower than previously estimated for LG (Lawson, Wadham, et al., 2014). However, scaling to GrIS runoff, total average annual DOC flux between 2007 and 2016 (Bamber et al., 2018) was 0.065 ± 0.010 Tg C $year^{-1}$, similar to previous estimates made for runoff from the GrIS (Bhatia et al., 2013; Hood et al., 2015). These studies used higher average DOC concentrations for glacial meltwaters but calculated fluxes for the 1961–1990 reference period when glacial runoff in Greenland was not increasing (Bamber et al., 2012). While studies from other GrIS outlet glaciers are necessary for determining whether the seasonal pattern of DOC concentrations in LG outflow is representative of other GrIS glaciers (e.g., in terms of catchment size and location), these are the first estimates of annual DOC flux using GrIS runoff from 2007 to 2016 (Bamber et al., 2018), which is ~320 km^3 $year^{-1}$ greater than that of the 1961–1990 reference period (251 ± 50 km^3 $year^{-1}$) (Bamber et al., 2012). Finally, stochastic shifts in optical properties during the outburst and postoutburst periods describe a unique, previously unidentified source of DOM, with potential implications for downstream bioavailability, highlighting the utility of high-frequency, long-time-series sampling of glacial systems.

Acknowledgments
This research is part of a UK NERC-funded project (DELVE; NERC grant NE/I008845/1). Fieldwork was additionally supported by a Czech Science Foundation Junior Grant (GACR 15-17346Y) to M. S. J. R. H. was partially supported by the European Union's Horizon 2020 research and innovation program under the Marie Sklodowska-Curie Actions fellowship ICICLES (grant agreement 793962), and T. J. K. was supported by Charles University Research Centre program 204069. This work was also supported by the National Science Foundation grants OCE 1333157 and OCE 1464396 to R. G. M. S. The authors would like to thank all those involved in fieldwork at Leverett Camp, particularly E. Baghshaw, J. Telling, A. Tedstone, and G. Lamarche-Gagnon. We would additionally like to thank S. E. Johnston for assistance in the lab. Data can be found in Table 1 and the supporting information and are available through PANGAEA (https://doi.org/10.1594/PANGAEA.910920) and Kellerman et al. (2020).

References

Armbruster, D. A., & Pry, T. (2008). Limit of blank, limit of detection and limit of quantitation. *Clinical Biochemist Reviews*, *29*(Suppl 1), S49–S52.

Bamber, J. L., Broeke, M. V. D., Ettema, J., Lenaerts, J., & Rignot, E. (2012). Recent large increases in freshwater fluxes from Greenland into the North Atlantic. *Geophysical Research Letters*, *39*, L19501. https://doi.org/10.1029/2012gl052552

Bamber, J. L., Tedstone, A. J., King, M. D., Howat, I. M., Enderlin, E. M., Broeke, M. R. V. D., & Noel, B. (2018). Land ice freshwater budget of the Arctic and North Atlantic Oceans: 1. Data, methods, and results. *Journal of Geophysical Research: Oceans*, *123*, 1827–1837. https://doi.org/10.1002/2017JC013605

Barker, J. D., Dubnick, A., Lyons, W. B., & Chin, Y. P. (2013). Changes in dissolved organic matter (DOM) fluorescence in proglacial Antarctic streams. *Arctic, Antarctic, and Alpine Research*, *45*(3), 305–317. https://doi.org/10.1657/1938-4246-45.3.305

Bartholomew, I., Nienow, P., Sole, A., Mair, D., Cowton, T., Palmer, S., & Wadham, J. (2011). Supraglacial forcing of subglacial drainage in the ablation zone of the Greenland Ice Sheet. *Geophysical Research Letters*, *38*, L08502. https://doi.org/10.1029/2011gl047063

Beaton, A. D., Wadham, J. L., Hawkings, J., Bagshaw, E. A., Lamarche-Gagnon, G., Mowlem, M. C., & Tranter, M. (2017). High-resolution in situ measurement of nitrate in runoff from the Greenland Ice Sheet. *Environmental Science & Technology*, *51*(21), 12,518–12,527. https://doi.org/10.1021/acs.est.7b03121

Belzile, C., Gibson, J. A. E., & Vincent, W. F. (2002). Colored dissolved organic matter and dissolved organic carbon exclusion from lake ice: Implications for irradiance transmission and carbon cycling. *Limnology and Oceanography*, *47*(5), 1283–1293. https://doi.org/10.4319/lo.2002.47.5.1283

Bhatia, M. P., Das, S. B., Kujawinski, E. B., Henderson, P., Burke, A., & Charette, M. A. (2011). Seasonal evolution of water contributions to discharge from a Greenland outlet glacier: Insight from a new isotope-mixing model. *Journal of Glaciology*, *57*(205), 929–941. https://doi.org/10.3189/002214311798043861

Bhatia, M. P., Das, S. B., Longnecker, K., Charette, M. A., & Kujawinski, E. B. (2010). Molecular characterization of dissolved organic matter associated with the Greenland Ice Sheet. *Geochimica et Cosmochimica Acta*, *74*(13), 3768–3784. https://doi.org/10.1016/j.gca.2010.03.035

Bhatia, M. P., Das, S. B., Xu, L., Charette, M. A., Wadham, J. L., & Kujawinski, E. B. (2013). Organic carbon export from the Greenland Ice Sheet. *Geochimica et Cosmochimica Acta*, *109*, 329–344. https://doi.org/10.1016/j.gca.2013.02.006

Birdwell, J. E., & Engel, A. S. (2009). Variability in terrestrial and microbial contributions to dissolved organic matter fluorescence in the Edwards Aquifer, Central Texas. *Journal of Cave and Karst Studies*, *71*(2), 144–156.

Braithwaite, R. J. (1995). Positive degree-day factors for ablation on the Greenland Ice Sheet studied by energy-balance modelling. *Journal of Glaciology*, *41*(137), 153–160.

Cameron, K. A., Stibal, M., Hawkings, J. R., Mikkelsen, A. B., Telling, J., Kohler, T. J., et al. (2017). Meltwater export of prokaryotic cells from the Greenland Ice Sheet. *Environmental Microbiology*, *19*(2), 524–534. https://doi.org/10.1111/1462-2920.13483

Chandler, D. M., Wadham, J. L., Lis, G. P., Cowton, T., Sole, A., Bartholomew, I., et al. (2013). Evolution of the subglacial drainage system beneath the Greenland Ice Sheet revealed by tracers. *Nature Geoscience*, *6*(3), 195–198. https://doi.org/10.1038/ngeo1737

Chen, Y., Wu, L., Boden, R., Hillebrand, A., Kumaresan, D., Moussard, H., et al. (2009). Life without light: Microbial diversity and evidence of sulfur- and ammonium-based chemolithotrophy in Movile Cave. *The ISME Journal*, *3*(9), 1093–1104. https://doi.org/10.1038/ismej.2009.57

Christiansen, J. R., & Jorgensen, C. J. (2018). First observation of direct methane emission to the atmosphere from the subglacial domain of the Greenland Ice Sheet. *Scientific Reports*, *8*(1), 16,623. https://doi.org/10.1038/s41598-018-35054-7

Christoffersen, P., Bougamont, M., Hubbard, A., Doyle, S. H., Grigsby, S., & Pettersson, R. (2018). Cascading lake drainage on the Greenland Ice Sheet triggered by tensile shock and fracture. *Nature Communications*, *9*(1), 1–12. https://doi.org/10.1038/s41467-018-03420-8

Clason, C. C., Mair, D. W. F., Nienow, P. W., Bartholomew, I. D., Sole, A., Palmer, S., & Schwanghart, W. (2015). Modelling the transfer of supraglacial meltwater to the bed of Leverett Glacier, Southwest Greenland. *The Cryosphere*, *9*(1), 123–138. https://doi.org/10.5194/tc-9-123-2015

Cook, J. M., Hodson, A. J., Anesio, A. M., Hanna, E., Yallop, M., Stibal, M., et al. (2017). An improved estimate of microbially mediated carbon fluxes from the Greenland Ice Sheet. *Journal of Glaciology*, *58*(212), 1098–1108. https://doi.org/10.3189/2012JoG12J001

Cowton, T., Nienow, P., Bartholomew, I., Sole, A., & Mair, D. (2012). Rapid erosion beneath the Greenland Ice Sheet. *Geology*, *40*(4), 343–346. https://doi.org/10.1130/g32687.1

Dieser, M., Broemsen, E. L., Cameron, K. A., King, G. M., Achberger, A., Choquette, K., et al. (2014). Molecular and biogeochemical evidence for methane cycling beneath the western margin of the Greenland Ice Sheet. *The ISME Journal*, *8*(11), 2305–2316. https://doi.org/10.1038/ismej.2014.59

Dow, C. F., Kulessa, B., Rutt, I. C., Tsai, V. C., Pimentel, S., Doyle, S. H., et al. (2015). Modeling of subglacial hydrological development following rapid supraglacial lake drainage. *Journal of Geophysical Research: Earth Surface*, *120*, 1127–1147. https://doi.org/10.1002/2014JF003333

Dubnick, A., Barker, J., Sharp, M., Wadham, J., Lis, G., Telling, J., et al. (2017). Characterization of dissolved organic matter (DOM) from glacial environments using total fluorescence spectroscopy and parallel factor analysis. *Annals of Glaciology*, *51*(56), 111–122. https://doi.org/10.3189/172756411795931912

Fellman, J. B., Hood, E., Raymond, P. A., Stubbins, A., & Spencer, R. G. (2015). Spatial variation in the origin of dissolved organic carbon in snow on the Juneau Icefield, Southeast Alaska. *Environmental Science & Technology*, *49*(19), 11,492–11,499. https://doi.org/10.1021/acs.est.5b02685

Fellman, J. B., Hood, E., & Spencer, R. G. M. (2010). Fluorescence spectroscopy opens new windows into dissolved organic matter dynamics in freshwater ecosystems: A review. *Limnology and Oceanography*, *55*(6), 2452–2462.

Fellman, J. B., Spencer, R. G. M., Hernes, P. J., Edwards, R. T., D'Amore, D. V., & Hood, E. (2010). The impact of glacier runoff on the biodegradability and biochemical composition of terrigenous dissolved organic matter in near-shore marine ecosystems. *Marine Chemistry*, *121*(1–4), 112–122. https://doi.org/10.1016/j.marchem.2010.03.009

Goncalves-Araujo, R., Granskog, M. A., Bracher, A., Azetsu-Scott, K., Dodd, P. A., & Stedmon, C. A. (2016). Using fluorescent dissolved organic matter to trace and distinguish the origin of Arctic surface waters. *Scientific Reports*, *6*(1), 1–12. https://doi.org/10.1038/srep33978

Hansell, D. A., Carlson, C. A., Repeta, D. J., & Schlitzer, R. (2009). Dissolved organic matter in the ocean a controversy stimulates new insights. *Oceanography*, *22*(4), 202–211. https://doi.org/10.5670/oceanog.2009.109

Harrold, Z. R., Skidmore, M. L., Hamilton, T. L., Desch, L., Amada, K., van Gelder, W., et al. (2015). Aerobic and anaerobic thiosulfate oxidation by a cold-adapted, subglacial chemoautotroph. *Applied and Environmental Microbiology*, *82*(5), 1486–1495. https://doi.org/10.1128/AEM.03398-15

Hatton, J. E., Hendry, K. R., Hawkings, J. R., Wadham, J. L., Kohler, T. J., Stibal, M., et al. (2019). Investigation of subglacial weathering under the Greenland Ice Sheet using silicon isotopes. *Geochimica et Cosmochimica Acta*, *247*, 191–206. https://doi.org/10.1016/j.gca.2018.12.033

Hawkings, J. R., Hatton, J. E., Hendry, K. R., de Souza, G. F., Wadham, J. L., Ivanovic, R., et al. (2018). The silicon cycle impacted by past ice sheets. *Nature Communications*, *9*(1), 3210. https://doi.org/10.1038/s41467-018-05689-1

Hawkings, J. R., Wadham, J., Tranter, M., Telling, J., Bagshaw, E., Beaton, A., et al. (2016). The Greenland Ice Sheet as a hot spot of phosphorus weathering and export in the Arctic. *Global Biogeochemical Cycles*, *30*, 191–210. https://doi.org/10.1002/2015gb005237

Hawkings, J. R., Wadham, J. L., Tranter, M., Lawson, E., Sole, A., Cowton, T., et al. (2015). The effect of warming climate on nutrient and solute export from the Greenland Ice Sheet. *Geochemical Perspectives Letters*, *94-104*, 94–104. https://doi.org/10.7185/geochemlet.1510

Hawkings, J. R., Wadham, J. L., Tranter, M., Raiswell, R., Benning, L. G., Statham, P. J., et al. (2014). Ice sheets as a significant source of highly reactive nanoparticulate iron to the oceans. *Nature Communications*, *5*, 3929. https://doi.org/10.1038/ncomms4929

Hedges, J. I. (1992). Global biogeochemical cycles: Progress and problems. *Marine Chemistry*, *39*(1), 67–93. https://doi.org/10.1016/0304-4203(92)90096-s

Hernes, P. J., Bergamaschi, B. A., Eckard, R. S., & Spencer, R. G. M. (2009). Fluorescence-based proxies for lignin in freshwater dissolved organic matter. *Journal of Geophysical Research*, *114*, G00F03. https://doi.org/10.1029/2009JG000938

Holland, A. T., Williamson, C. J., Sgouridis, F., Tedstone, A. J., McCutcheon, J., Cook, J. M., et al. (2019). Dissolved organic nutrients dominate melting surface ice of the Dark Zone (Greenland Ice Sheet). *Biogeosciences*, *16*(16), 3283–3296. https://doi.org/10.5194/bg-16-3283-2019

Hood, E., Battin, T. J., Fellman, J., O'Neel, S., & Spencer, R. G. M. (2015). Storage and release of organic carbon from glaciers and ice sheets. *Nature Geoscience*, *8*(2), 91–96. https://doi.org/10.1038/Ngeo2331

Hood, E., Fellman, J., Spencer, R. G., Hernes, P. J., Edwards, R., D'Amore, D., & Scott, D. (2009). Glaciers as a source of ancient and labile organic matter to the marine environment. *Nature*, *462*(7276), 1044–1047. https://doi.org/10.1038/nature08580

Jordan, T. M., Williams, C. N., Schroeder, D. M., Martos, Y. M., Cooper, M. A., Siegert, M. J., et al. (2018). A constraint upon the basal water distribution and thermal state of the Greenland Ice Sheet from radar bed echoes. *The Cryosphere*, *12*(9), 2831–2854. https://doi.org/10.5194/tc-12-2831-2018

Kellerman, A. M., Guillemette, F., Podgorski, D. C., Aiken, G. R., Butler, K. D., & Spencer, R. G. M. (2018). Unifying concepts linking dissolved organic matter composition to persistence in aquatic ecosystems. *Environmental Science & Technology*, *52*(5), 2538–2548. https://doi.org/10.1021/acs.est.7b05513

Kellerman, A. M., Hawkings, J. R., Wadham, J. L., Kohler, T. J., Stibal, M., Grater, E., et al. (2020). Fluorescence properties of dissolved organic matter from Leverett Glacier outflow. *Pangaea*. https://doi.org/10.1594/PANGAEA.910920

Kellerman, A. M., Kothawala, D. N., Dittmar, T., & Tranvik, L. J. (2015). Persistence of dissolved organic matter in lakes related to its molecular characteristics. *Nature Geoscience*, *8*(6), 454–457. https://doi.org/10.1038/ngeo2440

Knight, P. G. (1997). The basal ice layer of glaciers and ice sheets. *Quaternary Science Reviews*, *16*(9), 975–993. https://doi.org/10.1016/S0277-3791(97)00033-4

Kohler, T. J., Zarsky, J. D., Yde, J. C., Lamarche-Gagnon, G., Hawkings, J. R., Tedstone, A. J., et al. (2017). Carbon dating reveals a seasonal progression in the source of particulate organic carbon exported from the Greenland Ice Sheet. *Geophysical Research Letters*, *44*, 6209–6217. https://doi.org/10.1002/2017gl073219

Kothawala, D. N., Stedmon, C. A., Muller, R. A., Weyhenmeyer, G. A., Kohler, S. J., & Tranvik, L. J. (2014). Controls of dissolved organic matter quality: Evidence from a large-scale boreal lake survey. *Global Change Biology*, *20*(4), 1101–1114. https://doi.org/10.1111/gcb.12488

Lamarche-Gagnon, G., Wadham, J. L., Sherwood Lollar, B., Arndt, S., Fietzek, P., Beaton, A. D., et al. (2019). Greenland melt drives continuous export of methane from the ice-sheet bed. *Nature*, *565*(7737), 73–77. https://doi.org/10.1038/s41586-018-0800-0

Lawson, E. C., Bhatia, M. P., Wadham, J. L., & Kujawinski, E. B. (2014). Continuous summer export of nitrogen-rich organic matter from the Greenland Ice Sheet inferred by ultrahigh resolution mass spectrometry. *Environmental Science & Technology*, *48*(24), 14248–14257. https://doi.org/10.1021/es501732h

Lawson, E. C., Wadham, J. L., Tranter, M., Stibal, M., Lis, G. P., Butler, C. E. H., et al. (2014). Greenland Ice Sheet exports labile organic carbon to the Arctic oceans. *Biogeosciences*, *11*(14), 4015–4028. https://doi.org/10.5194/bg-11-4015-2014

Lecavalier, B. S., Milne, G. A., Simpson, M. J. R., Wake, L., Huybrechts, P., Tarasov, L., et al. (2014). A model of Greenland Ice Sheet deglaciation constrained by observations of relative sea level and ice extent. *Quaternary Science Reviews*, *102*, 54–84. https://doi.org/10.1016/j.quascirev.2014.07.018

Levy, L. B., Larsen, N. K., Davidson, T. A., Strunk, A., Olsen, J., & Jeppesen, E. (2017). Contrasting evidence of Holocene ice margin retreat, south-western Greenland. *Journal of Quaternary Science*, *32*(5), 604–616. https://doi.org/10.1002/jqs.2957

Lindback, K., Pettersson, R., Hubbard, A. L., Doyle, S. H., van As, D., Mikkelsen, A. B., & Fitzpatrick, A. A. (2015). Subglacial water drainage, storage, and piracy beneath the Greenland Ice Sheet. *Geophysical Research Letters*, *42*, 7606–7614. https://doi.org/10.1002/2015gl065393

MacGregor, J. A., Fahnestock, M. A., Catania, G. A., Aschwanden, A., Clow, G. D., Colgan, W. T., et al. (2016). A synthesis of the basal thermal state of the Greenland Ice Sheet. *Journal of Geophysical Research: Earth Surface*, *121*, 1328–1350. https://doi.org/10.1002/2015jf003803

Maie, N., Scully, N. M., Pisani, O., & Jaffe, R. (2007). Composition of a protein-like fluorophore of dissolved organic matter in coastal wetland and estuarine ecosystems. *Water Research*, *41*(3), 563–570. https://doi.org/10.1016/j.watres.2006.11.006

Martinez-Perez, A. M., Nieto-Cid, M., Osterholz, H., Catala, T. S., Reche, I., Dittmar, T., & Alvarez-Salgado, X. A. (2017). Linking optical and molecular signatures of dissolved organic matter in the Mediterranean Sea. *Scientific Reports*, *7*(1), 3436. https://doi.org/10.1038/s41598-017-03735-4

McKnight, D. M., Boyer, E. W., Westerhoff, P. K., Doran, P. T., Kulbe, T., & Andersen, D. T. (2001). Spectrofluorometric characterization of dissolved organic matter for indication of precursor organic material and aromaticity. *Limnology and Oceanography*, *46*(1), 38–48. https://doi.org/10.4319/lo.2001.46.1.0038

Murphy, K. R., Stedmon, C. A., Graeber, D., & Bro, R. (2013). Fluorescence spectroscopy and multi-way techniques. PARAFAC. *Analytical Methods*, *5*(23), 6557–6566. https://doi.org/10.1039/C3ay41160e

Murphy, K. R., Stedmon, C. A., Wenig, P., & Bro, R. (2014). OpenFluor—An online spectral library of auto-fluorescence by organic compounds in the environment. *Analytical Methods*, *6*(3), 658–661. https://doi.org/10.1039/C3ay41935e

Musilova, M., Tranter, M., Wadham, J., Telling, J., Tedstone, A., & Anesio, A. M. (2017). Microbially driven export of labile organic carbon from the Greenland Ice Sheet. *Nature Geoscience*, *10*(5), 360–365. https://doi.org/10.1038/Ngeo2920

Nienow, P. W., Sole, A. J., Slater, D. A., & Cowton, T. R. (2017). Recent advances in our understanding of the role of Meltwater in the Greenland Ice Sheet system. *Current Climate Change Reports*, *3*(4), 330–344. https://doi.org/10.1007/s40641-017-0083-9

O'Donnell, E. C., Wadham, J. L., Lis, G. P., Tranter, M., Pickard, A. E., Stibal, M., et al. (2016). Identification and analysis of low-molecular-weight dissolved organic carbon in subglacial basal ice ecosystems by ion chromatography. *Biogeosciences*, *13*(12), 3833–3846. https://doi.org/10.5194/bg-13-3833-2016

Oksanen, J., Blanchet, F. G., Kindt, R., Legender, P., Minchin, P. R., O'Hara, R. B., et al. (2011). vegan: Community ecology package. R package version 2.0–0, edited.

Osburn, C. L., Boyd, T. J., Montgomery, M. T., Bianchi, T. S., Coffin, R. B., & Paerl, H. W. (2016). Optical proxies for terrestrial dissolved organic matter in estuaries and coastal waters. *Frontiers in Marine Science*, *2*, 127. https://doi.org/10.3389/fmars.2015.00127

Osburn, C. L., Handsel, L. T., Peierls, B. L., & Paerl, H. W. (2016). Predicting sources of dissolved organic nitrogen to an estuary from an agro-urban coastal watershed. *Environmental Science & Technology*, *50*(16), 8473–8484. https://doi.org/10.1021/acs.est.6b00053

Paulsen, M. L., Nielsen, S. E. B., Müller, O., Møller, E. F., Stedmon, C.A., Juul-Pedersen, T., et al. (2017). Carbon bioavailability in a high arctic fjord influenced by glacial meltwater, NE Greenland. *Frontiers in Marine Science*, *4*(176). https://doi.org/10.3389/fmars.2017.00176

Petsch, S. T., Edwards, K. J., & Eglinton, T. I. (2005). Microbial transformations of organic matter in black shales and implications for global biogeochemical cycles. *Palaeogeography, Palaeoclimatology, Palaeoecology*, *219*(1–2), 157–170. https://doi.org/10.1016/j.palaeo.2004.10.019

Petsch, S. T., Eglington, T. I., & Edwards, K. J. (2001). 14C-dead living biomass: Evidence for microbial assimilation of ancient organic carbon during shale weathering. *Science*, *292*(5519), 1127–1131. https://doi.org/10.1126/science.1058332

R Core Team (2015). R: A language and environment for statistical computing. R Foundation for Statistical Computing, Vienna, Austria.

Remias, D., Schwaiger, S., Aigner, S., Leya, T., Stuppner, H., & Lutz, C. (2012). Characterization of an UV- and VIS-absorbing, purpurogallin-derived secondary pigment new to algae and highly abundant in *Mesotaenium berggrenii* (*Zygnematophyceae*, Chlorophyta), an extremophyte living on glaciers. *FEMS Microbiology Ecology*, *79*(3), 638–648. https://doi.org/10.1111/j.1574-6941.2011.01245.x

Shepherd, A., Ivins, E. R., A, G., Barletta, V. R., Bentley, M. J., Bettadpur, S., et al. (2012). A reconciled estimate of ice-sheet mass balance. *Science*, *338*(6111), 1183–1189. https://doi.org/10.1126/science.1228102

Simpson, M. J. R., Milne, G. A., Huybrechts, P., & Long, A. J. (2009). Calibrating a glaciological model of the Greenland Ice Sheet from the Last Glacial Maximum to present-day using field observations of relative sea level and ice extent. *Quaternary Science Reviews*, *28*(17–18), 1631–1657. https://doi.org/10.1016/j.quascirev.2009.03.004

Singer, G. A., Fasching, C., Wilhelm, L., Niggemann, J., Steier, P., Dittmar, T., & Battin, T. J. (2012). Biogeochemically diverse organic matter in Alpine glaciers and its downstream fate. *Nature Geoscience*, *5*(10), 710–714. https://doi.org/10.1038/Ngeo1581

Smith, H. J., Dieser, M., McKnight, D. M., SanClements, M. D., & Foreman, C. M. (2018). Relationship between dissolved organic matter quality and microbial community composition across polar glacial environments. *FEMS Microbiology Ecology*, *94*(7), fiy090. https://doi.org/10.1093/femsec/fiy090

Smith, H. J., Foster, R. A., McKnight, D. M., Lisle, J. T., Littmann, S., Kuypers, M. M. M., & Foreman, C. M. (2017). Microbial formation of labile organic carbon in Antarctic glacial environments. *Nature Geoscience*, *10*(5), 356–359. https://doi.org/10.1038/Ngeo2925

Smith, L. C., Chu, V. W., Yang, K., Gleason, C. J., Pitcher, L. H., Rennermalm, A. K., et al. (2015). Efficient meltwater drainage through supraglacial streams and rivers on the southwest Greenland Ice Sheet. *Proceedings of the National Academy of Sciences of the United States of America*, *112*(4), 1001–1006. https://doi.org/10.1073/pnas.1413024112

Sole, A., Nienow, P., Bartholomew, I., Mair, D., Cowton, T., Tedstone, A., & King, M. A. (2013). Winter motion mediates dynamic response of the Greenland Ice Sheet to warmer summers. *Geophysical Research Letters*, *40*, 3940–3944. https://doi.org/10.1002/grl.50764

Spencer, R. G. M., Aiken, G. R., Dornblaser, M. M., Butler, K. D., Holmes, R. M., Fiske, G., et al. (2013). Chromophoric dissolved organic matter export from U.S. rivers. *Geophysical Research Letters*, *40*, 1575–1579. https://doi.org/10.1002/grl.50357

Spencer, R. G. M., & Coble, P. G. (2014). *Sampling design for organic matter fluorescence analysis*, *Camb Env Ch*, edited (pp. 125–146). Cambridge University Press. https://doi.org/10.1017/Cbo9781139045452

Spencer, R. G. M., Guo, W. D., Raymond, P. A., Dittmar, T., Hood, E., Fellman, J., & Stubbins, A. (2014). Source and biolability of ancient dissolved organic matter in glacier and lake ecosystems on the Tibetan Plateau. *Geochimica et Cosmochimica Acta*, *142*, 64–74. https://doi.org/10.1016/j.gca.2014.08.006

Spencer, R. G. M., Vermilyea, A., Fellman, J., Raymond, P., Stubbins, A., Scott, D., & Hood, E. (2014). Seasonal variability of organic matter composition in an Alaskan glacier outflow: Insights into glacier carbon sources. *Environmental Research Letters*, *9*(5). https://doi.org/10.1088/1748-9326/9/5/055005

Stibal, M., Wadham, J. L., Lis, G. P., Telling, J., Pancost, R. D., Dubnick, A., et al. (2012). Methanogenic potential of Arctic and Antarctic subglacial environments with contrasting organic carbon sources. *Global Change Biology*, *18*(11), 3332–3345. https://doi.org/10.1111/j.1365-2486.2012.02763.x

Stubbins, A., Hood, E., Raymond, P. A., Aiken, G. R., Sleighter, R. L., Hernes, P. J., et al. (2012). Anthropogenic aerosols as a source of ancient dissolved organic matter in glaciers. *Nature Geoscience*, *5*(3), 198–201. https://doi.org/10.1038/Ngeo1403

Stubbins, A., Lapierre, J. F., Berggren, M., Prairie, Y. T., Dittmar, T., & del Giorgio, P. A. (2014). What's in an EEM? Molecular signatures associated with dissolved organic fluorescence in boreal Canada. *Environmental Science & Technology*, *48*(18), 10,598–10,606. https://doi.org/10.1021/es502086e

Tedesco, M., Fettweis, X., Mote, T., Wahr, J., Alexander, P., Box, J. E., & Wouters, B. (2013). Evidence and analysis of 2012 Greenland records from spaceborne observations, a regional climate model and reanalysis data. *The Cryosphere*, *7*(2), 615–630. https://doi.org/10.5194/tc-7-615-2013

Trusel, L. D., Das, S. B., Osman, M. B., Evans, M. J., Smith, B. E., Fettweis, X., et al. (2018). Nonlinear rise in Greenland runoff in response to post-industrial Arctic warming. *Nature*, *564*(7734), 104–108. https://doi.org/10.1038/s41586-018-0752-4

van den Broeke, M. R., Enderlin, E. M., Howat, I. M., Munneke, P. K., Noel, B. P. Y., van de Berg, W. J., et al. (2016). On the recent contribution of the Greenland Ice Sheet to sea level change. *The Cryosphere*, *10*(5), 1933–1946. https://doi.org/10.5194/tc-10-1933-2016

Wadham, J. L., Hawkings, J., Telling, J., Chandler, D., Alcock, J., O'Donnell, E., et al. (2016). Sources, cycling and export of nitrogen on the Greenland Ice Sheet. *Biogeosciences*, *13*(22), 6339–6352. https://doi.org/10.5194/bg-13-6339-2016

Wadham, J. L., Tranter, M., Tulaczyk, S., & Sharp, M. (2008). Subglacial methanogenesis: A potential climatic amplifier? *Global Biogeochemical Cycles*, *22*, GB2021. https://doi.org/10.1029/2007gb002951

Williamson, C. J., Anesio, A. M., Cook, J., Tedstone, A., Poniecka, E., Holland, A., et al. (2018). Ice algal bloom development on the surface of the Greenland Ice Sheet. *FEMS Microbiology Ecology*, *94*(3), fiy025. https://doi.org/10.1093/femsec/fiy025

Wünsch, U. J., Murphy, K. R., & Stedmon, C. A. (2017). The one-sample PARAFAC approach reveals molecular size distributions of fluorescent components in dissolved organic matter. *Environmental Science & Technology*, *51*(20), 11,900–11,908. https://doi.org/10.1021/acs.est.7b03260

Yde, J. C., Finster, K. W., Raiswell, R., Steffensen, J. P., Heinemeier, J., Olsen, J., et al. (2010). Basal ice microbiology at the margin of the Greenland Ice Sheet. *Annals of Glaciology*, *51*(56), 71–79. https://doi.org/10.3189/172756411795931976